



Mechanical behavior of multilayer graphene reinforced epoxy nano-composites via a hierarchical multi-scale technique

H. Ahmadi^a, M. Jahanshahi^a, A.R. Khoei^{b,*}, S. Bordas^{c,d}

^a Department of Civil Engineering, School of Science and Engineering, Sharif University of Technology, International Campus, P.O. Box 76417-76655, Kish Island, Iran

^b Center of Excellence in Structures and Earthquake Engineering, Department of Civil Engineering, Sharif University of Technology, P.O. Box 11365-9313, Tehran, Iran

^c Institute of Computational Engineering, University of Luxembourg, 6 Avenue de la Fonte, 4362 Esch-sur-Alzette, Luxembourg

^d Institute of Theoretical, Applied and Computational Mechanics, Cardiff University, Cardiff CF24 3AA, United Kingdom

ARTICLE INFO

Article history:

Received 21 February 2021

Revised 29 March 2021

Accepted 30 March 2021

Keywords:

Graphene sheets

Epoxy resin

Hyperelasticity

Multi-scale method

Molecular dynamics simulation

ABSTRACT

In this paper, a multi-scale technique is presented to study the mechanical behavior of nano-composites by linking the atomistic information from lower scale to the continuum model in upper scale. Molecular dynamics simulations are employed to compute the material properties of graphene/epoxy nano-composites using the COMPASS interatomic force field. In order to obtain the atomistic stress surfaces used to evaluate the mechanical properties of material in upper scale, the biaxial loading is applied to different representative volume elements. On the continuum level, the hyperelastic strain energy functions are utilized to calculate the material parameters using the hyperelastic functions from atomistic data. The stress and elasticity tensors are obtained by computing the first and second order derivatives of hyperelastic functions with reference to the components of the right Cauchy–Green deformation tensor. The stress–strain surfaces of hyperelastic functions in lower scale are used to calculate the properties of nano-composite material in upper scale. The efficiency and applicability of the proposed technique is presented through various numerical examples. It is shown that the proposed multi-scale technique is able to solve large problems within acceptable computational time, which is not possible using conventional molecular dynamics approaches.

Crown Copyright © 2021 Published by Elsevier Ltd.
This is an open access article under the CC BY-NC-ND license
(<http://creativecommons.org/licenses/by-nc-nd/4.0/>)

1. Introduction

The exceptional properties of carbon nano-composites and their application in aerospace structures have attracted attention in last decades [1–3]. Epoxy resins are widely used matrix materials, which depict good mechanical properties and thermal stability in different applications [4]. Various investigations have proven that reinforcing epoxy with graphene could potentially enhance the mechanical properties of pure epoxy [5–7]. There are indications that increasing the number of graphene nano-plates (GNP) could improve the mechanical behavior of composite nano-materials [8]. Atomistic simulations are efficient computational tools for exploring the material behavior at atomic level. These powerful techniques have been used widely for modeling the mechanical response of complex nano-structures [9–17]. Rahman and Haque

[18] studied the interfacial properties and elastic modulus of cross linked graphene reinforced epoxy using molecular dynamics (MD) simulations. The mechanical and thermal characteristics of epoxy reinforced with different graphene materials such as pure, oxide and flakes were proposed by Shiu and Tsai [19] based on MD simulation. Moreover, Li et al. [20] employed MD analyses to evaluate the effect of multilayer graphene sheets on the mechanical properties of graphene/epoxy nano-composite. Li et al. [21] carried out MD simulations to study thermal characteristics of defective graphene/epoxy nano-composite. Atomistic simulations are computationally costly and, hence, are applicable for small specimens with limited number of atoms. The continuum methods do not possess sufficient accuracy to depict atomic interactions in complex nano-structures. To overcome these drawbacks, different multi-scale techniques, such as hierarchical and concurrent methods, have been developed by the researchers to correlate the atomistic and continuum models [22, 23].

* Corresponding author.

E-mail address: arkhoei@sharif.edu (A.R. Khoei).

The Cauchy–Born (CB) hypothesis is a standard approach to link the atomistic data in nano-structures to the continuum domain [24, 25]. This hypothesis has been employed in many multi-scale approaches, such as quasi-continuum, bridging scale and CG-MD methods [26–29], to bridge the atomic information in lower scale to the continuum model in upper scale. Khoei et al. [30] discussed the validity of CB hypothesis for Sutton–Chen potential by comparing atomistic information and continuum results. Furthermore, Shahabodini et al. [31] presented higher order CB rule for flexural behavior of graphene sheets by correlating the Tersoff–Brenner interatomic potential and continuum strain energy. Khoei et al. [32] studied the validity of CB hypothesis in the presence of plastic deformations by providing a validity surface in stress space. Nevertheless, it is not a trivial task to simulate the nonlinear behavior of nano-structures using finite element method and CB hypothesis for complex interatomic potentials. The hyperelasticity continuum theory is considered as a widely used approach for describing the nonlinear behavior of various materials, such as polymers, soft materials and foams among others [33–35]. Different hyperelastic functions such as Fung, Neo-Hookean, Mooney–Rivlin, Ogden, and Polynomial have been developed by researchers for modeling the multi-scale response of nano-structures [36]. Saavedra Flores et al. [37] developed an Ogden-type hyperelastic function to investigate the buckling behavior of a single wall carbon nano-tube under axial compression. Arroyo and Belytschko [38] developed a hyperelastic membrane function for the carbon nano-tubes based on the atomistic model. They proposed an extension of the Cauchy–Born rule to predict the behavior of a single layer crystalline film. Applying the Ogden hyperelastic function and Tersoff–Brenner interatomic potential, the nonlinear response of single wall carbon nano-tubes in tension was studied by Saavedra Flores et al. [39]. The tensile response of graphene sheets using Ogden hyperelastic function was investigated by Saavedra Flores et al. [40]. Kim et al. [41] proposed polynomial-based hyperelastic functions that indicate the mechanical response of FCC and diamond cubic nano-structures. The continuum models were calculated via the application of various types of loadings to the specimens based on the Cauchy–Born hypothesis and fitting the continuum functions to the EAM and Tersoff potentials reference data. Jahanshahi et al. [42] employed the hyperelastic theory for multi-scale modeling of edge dislocations in various temperatures. In these and many other studies, the finite element method (FEM) has been employed as an efficient tool to discretize the domain in upper scale. Ahmadi et al. [43] and Hajikazemi et al. [44] used FEM to model the behavior of composite materials.

In the present paper, a hierarchical multi-scale technique is proposed to analyze the mechanical response of graphene reinforced epoxy based on bridging the atomistic simulations in lower scale to the continuum domain in upper scale. The stress–strain response of representative volume elements is obtained for nano-composites including multilayers of graphene sheets using molecular dynamics simulations. In order to link the atomistic simulation data to continuum models, the hyperelastic functions are employed to describe the mechanical behavior of atomistic description. The functions are obtained by applying the least squares procedure to fit the material models to atomistic data. As the most important feature of the technique, the time consuming molecular dynamics simulations in lower scale are replaced with hyperelastic functions that learned the mechanical properties of nano-composites through the fitting procedure. Applying the hyperelastic strain energy functions, the material properties of complex nano-composites are computed in the Gauss points of finite elements in upper scale. The proposed multiscale technique is especially applicable for GNP/epoxy matrices reinforced with carbon fibers. In this case, the elastic properties as derived in current research can be used to model the properties of randomly dis-

tributed GNP/epoxy cells containing short fibers at microscale. It is possible to implement the multiscale approach presented here to efficiently model the properties of these randomly distributed GNP/epoxy cells. It is only necessary to consider various continuity constraints between the cells. The article is organized as follows; Section 2 presents the molecular dynamics simulation of graphene/epoxy nano-composites. The details of COMPASS potential that is employed to model the material are presented in this section. Also, the challenges of modeling epoxy/graphene nano-composite are discussed. The theory of hyperelasticity is described in Section 3, and the parameters of polynomial hyperelastic function applied to learn the mechanical properties of graphene/epoxy nano-composite are discussed. Section 4 demonstrates the results of atomistic simulations and fitting procedure. The accuracy of developed hyperelastic functions to capture the behavior of nano-composite in lower scale is studied in this section. The performance of the proposed technique is investigated through various multi-scale examples in Section 5. Finally, some concluding remarks are derived in Section 6.

2. Atomistic analysis

In order to study the mechanical behavior of nano-composites at atomistic level, the molecular dynamics (MD) analysis is employed. The representative volume elements (RVEs) of epoxy reinforced with graphene sheets are used to investigate the elastic properties of the material. The COMPASS force field [45] has been chosen to calculate the total strain energy and to predict the mechanical behavior of material subject to different loading conditions. The total strain energy of the COMPASS force field includes different terms, such as the bond, angle, torsion angle, out-of-plane angle, cross-coupling parts, Coulomb function and 9-6 Lennard-Jones potential. This function can be defined as

$$E_{\text{total}} = E_b + E_\theta + E_\phi + E_\chi + E_{bb'} + E_{b\theta} + E_{b\phi} + E_{\theta\theta'} + E_{\theta\theta'\phi} + E_{\text{elec}} + E_{\text{LJ}} \quad (1)$$

$$E_b = \sum_b [K_2(b - b_0)^2 + K_3(b - b_0)^3 + K_4(b - b_0)^4] \quad (2)$$

$$E_\theta = \sum_\theta [H_2(\theta - \theta_0)^2 + H_3(\theta - \theta_0)^3 + H_4(\theta - \theta_0)^4] \quad (3)$$

$$E_\phi = \sum_\phi [V_1(1 - \cos\phi) + V_2(1 - \cos2\phi) + V_3(1 - \cos3\phi)] \quad (4)$$

$$E_\chi = \sum_\chi K_\chi(\chi - \chi_0)^2 \quad (5)$$

$$E_{bb'} = \sum_{b,b'} F_{b,b'}(b - b_0)(b' - b'_0) \quad (6)$$

$$E_{b\theta} = \sum_{b,\theta} F_{b,\theta}(b - b_0)(\theta - \theta_0) \quad (7)$$

$$E_{b\phi} = \sum_{b,\phi} F_{b,\phi}(b - b_0) \left[F_{b,\phi}^{(1)}(1 - \cos\phi) + F_{b,\phi}^{(2)}(1 - \cos2\phi) + F_{b,\phi}^{(3)}(1 - \cos3\phi) \right] \quad (8)$$

$$E_{\theta\theta'} = \sum_{\theta,\theta'} F_{\theta,\theta'}(\theta - \theta_0)(\theta' - \theta'_0) \quad (9)$$

$$E_{\theta\theta'\phi} = \sum_{\theta,\theta',\phi} F_{\theta,\theta',\phi}(\theta - \theta_0)(\theta' - \theta'_0)\cos\phi \quad (10)$$

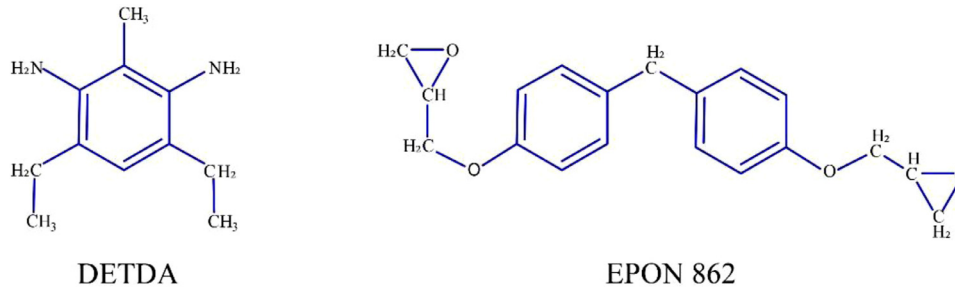


Fig. 1. Chemical structure of EPON 862 monomer and DETDA hardener [47].

$$E_{elec} = \sum_{i,j} \frac{q_i q_j}{\epsilon_0 r_{ij}} \quad (11)$$

$$E_{LJ} = \sum_{i,j} \epsilon_{ij} \left[2 \left(\frac{r_{ij}^0}{r_{ij}} \right)^9 - 3 \left(\frac{r_{ij}^0}{r_{ij}} \right)^6 \right] \quad (12)$$

where the parameters $r_{i,j}^0$ and ϵ_{ij} , appearing in 9-6 Lennard-Jones energy term can be calculated using the 6th order combination law as

$$r_{i,j}^0 = \left[\frac{(r_i^0)^6 + (r_j^0)^6}{2} \right]^{\frac{1}{6}} \quad (13)$$

$$\epsilon_{ij} = 2 \sqrt{\epsilon_i \epsilon_j} \left[\frac{(r_i^0)^3 (r_j^0)^3}{(r_i^0)^6 (r_j^0)^6} \right]^{\frac{1}{6}} \quad (14)$$

and the partial charge q_i for i th atom can be obtained by adding all charge bond increments δ_{ij} as

$$q_i = \sum_j \delta_{ij} \quad (15)$$

The parameters of COMPASS potential are described with sufficient details in Ref. [45].

During the MD simulations, the Nose-Hoover thermostat has been utilized to control the temperature of the system. To exclude thermal effects on final results, the temperature is set to 1 K. It is, however, an easy task to consider other values for temperature by performing the MD simulations at desired temperature and accomplishing the fitting procedure for new MD results. In order to construct the initial configuration of nano-composites, the Materials Studio software package has been employed in which all MD simulations are performed using LAMMPS (Large Scale Atomic/Molecular Massively Parallel Simulator) program [46]. The primary epoxy structures are created using EPON862 monomer (Di-glycidyl ether of Bisphenol-F) and DETDA hardener (Diethylene Toluene Diamine), as indicated in Fig. 1. In addition, the masses are specified for the atomic structures and periodic boundary conditions are employed for the system. The ratio of EPON862 and DETDA is considered as 2 : 1 for an epoxy molecule. Therefore, the total number of atoms in the epoxy molecule is equal to 83. In order to minimize internal forces, the molecular static minimization and molecular dynamic relaxation are applied using NVT ensemble. After minimizing the forces, the epoxy molecule is randomly distributed in the system. The multilayer graphene sheets have been embedded into the system to build the graphene/epoxy nano-composite. The dimensions of initial configuration are assumed as $52 \times 52 \times 76 \text{ \AA}$, where the cutoff radius of the van der Waals interaction corresponds to 10 \AA . After creating the initial configuration of nano-composite, the structure is relaxed by the molecular minimization and MD simulation. Applying the

fix/deform command in LAMMPS, a deformation is applied in z -direction to attain a density of 1.17 g/cc for the graphene/epoxy nano-composite. A molecular dynamics simulation with the NVT ensemble is employed to keep the volume and temperature constant during densification. In order to decrease the initial stress of condensed specimen, the NPT ensemble is used during the loading phase. A cross-linked density of 80% is considered for all RVEs so that the final thickness of epoxy layer remains close to 20 \AA .

It is worthwhile to mention that the density of 1.17 g/cc is achieved by applying several load steps along z -direction. In each load step, equal compressive deformations are applied to top and bottom boundaries of the specimen. Utilizing the load steps to decrease z -coordinates is to avoid large changes in the energy of the system due to packing the molecules too quickly. In the final specimen, the polymer layer extends about 13 \AA from both sides of graphene sheets. In this manner, it can be ensured that the interfacial region is fully captured and the effect of bulk polymer on the mechanical characteristics in xy -plane is minimized during the application of load in this plane. This approach has been described with sufficient details in Ref. [47].

3. Hyperelasticity model

Most atomistic structures illustrate the nonlinear behavior under different types of loading; it is a non-trivial task to use the interatomic potential based on the CB hypothesis in finite element analyses. Especially, the homogeneity of deformation gradient is lost at some stages of loading. Hyperelastic theory is a powerful continuum tool to describe the nonlinear response of material in large deformation regime. Based on this theory, the material response is path-independent and the stress in material can be derived from a strain energy function. Hyperelasticity can be used efficiently in modeling the atomistic behavior of material in lower scale. Hence, time consuming MD simulations are avoided in lower scale by properly learning the behavior of material at atomistic level. Hyperelastic models are used to relate the stress and strain based on material models, which are derived using a fitting procedure. The strain energy function ψ can be expressed using the invariants of the right Cauchy-Green deformation tensor.

The deformation gradient is used to link the position in reference configuration to the one in spatial configurations by

$$\mathbf{F} = \frac{\partial \mathbf{x}}{\partial \mathbf{X}} \quad (16)$$

Considering the material invariance, under superposed rigid body rotation, the strain energy function can be expressed as

$$\psi = \psi(I_1(\mathbf{C}), I_2(\mathbf{C}), I_3(\mathbf{C})) \quad (17)$$

where $\mathbf{C} = \mathbf{F}^T \mathbf{F}$ is the right Cauchy-Green deformation tensor, and I_1 , I_2 and I_3 are the invariants of \mathbf{C} , defined as

$$I_1 = \text{tr} \mathbf{C} \quad (18)$$

$$I_2 = \frac{1}{2} \{ (\text{tr} \mathbf{C})^2 - \text{tr} \mathbf{C}^2 \} \quad (19)$$

$$I_3 = \det \mathbf{C} = J^2 \quad (20)$$

where $J = \det \mathbf{F}$ is the volume change. The second Piola–Kirchhoff stress can be calculated using the first order derivative of the strain energy function with respect to the right Cauchy–Green deformation tensor as

$$\mathbf{S} = 2 \frac{\partial \psi(\mathbf{C})}{\partial \mathbf{C}} \quad (21)$$

Applying the second Piola–Kirchhoff stress, the Cauchy stress is determined by

$$\boldsymbol{\sigma} = \frac{1}{J} \mathbf{F} \mathbf{S} \mathbf{F}^T \quad (22)$$

The fourth order material elasticity tensor is computed according to the following relation as

$$\mathbf{C}^E = 4 \frac{\partial^2 \psi}{\partial \mathbf{C} \partial \mathbf{C}} \quad (23)$$

In continuum mechanics, it is conventional to decompose the deformation gradient into the volumetric and isochoric (volume preserving) parts as

$$\mathbf{F} = \mathbf{F}_{\text{vol}} \mathbf{F}' = J^{\frac{1}{3}} \mathbf{I} \mathbf{F}' \quad (24)$$

Accordingly, the right Cauchy–Green deformation can be expressed as

$$\mathbf{C} = \mathbf{C}_{\text{vol}} \mathbf{C}' \quad (25)$$

where

$$\mathbf{C}_{\text{vol}} = J^{\frac{2}{3}} \mathbf{I} \quad (26)$$

which represents the volumetric part of the right Cauchy–Green deformation tensor. In other words, it represents volume expansion or contraction; there is no pointwise distortion for \mathbf{C}_{vol} . In accordance with the right Cauchy–Green deformation tensor, the strain energy function can be decomposed into volumetric and isochoric parts as

$$\psi = \psi_D(I'_1, I'_2) + \psi_{\text{vol}}(J) \quad (27)$$

where the first and second invariants of isochoric \mathbf{C}' are calculated by

$$I'_1 = J^{-\frac{2}{3}} I_1 = \text{tr} \mathbf{C}' \quad (28)$$

$$I'_2 = J^{-\frac{4}{3}} I_2 = \frac{1}{2} \{ (\text{tr} \mathbf{C}')^2 - \text{tr} \mathbf{C}'^2 \} \quad (29)$$

The Polynomial Hyperelastic model, which is based on the first and second modified invariants, has been used herein to describe the nonlinear behavior of material. The general form of the polynomial material model is as follows

$$\psi = C_{10}(I'_1 - 3) + C_{20}(I'_1 - 3)^2 + C_{30}(I'_1 - 3)^3 + C_{01}(I'_2 - 3) + C_{02}(I'_2 - 3)^2 + C_{03}(I'_2 - 3)^3 + \psi_{\text{vol}}(J) \quad (30)$$

where the volumetric energy $\psi_{\text{vol}}(J)$ is defined as

$$\psi_{\text{vol}}(J) = \frac{K_1}{2} (\ln J)^2 + \frac{K_2}{2} (J - 1)^2 + K_3 (J - \ln J - 1) + K_4 (J \ln J - J + 1) \quad (31)$$

In order to learn the polynomial strain energy function, the RVEs in lower scale undergo biaxial deformations along x - and y -directions. Hence, the deformation gradient that is imposed on

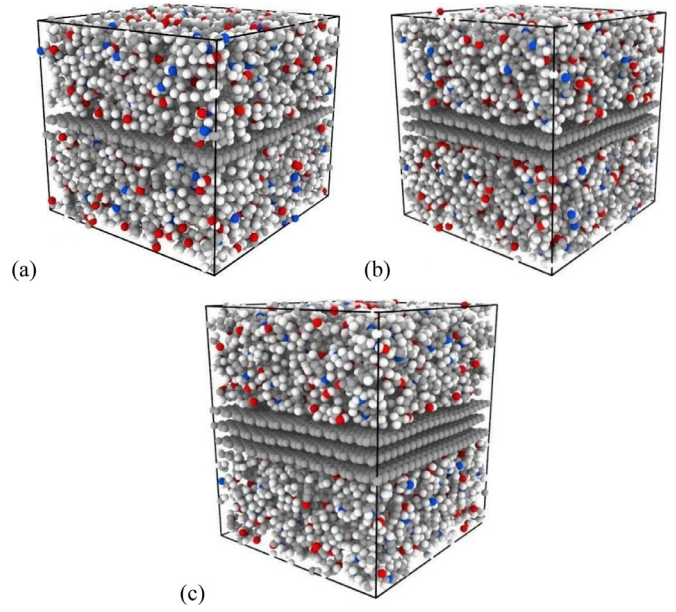


Fig. 2. The condensed structure of graphene/epoxy nanocomposites contains (a) one layer of graphene sheets, (b) two layers of graphene sheets and (c) three layers of graphene sheets. Gray, red, blue and white atoms represent carbon, oxygen, nitrogen and hydrogen, respectively.

the boundaries of the RVEs in each loading step takes the following form

$$\mathbf{F} = \begin{bmatrix} \lambda_1 & 0 & 0 \\ 0 & \lambda_2 & 0 \\ 0 & 0 & 1 \end{bmatrix} \quad (32)$$

where λ_1 and λ_2 are, respectively, the principal stretches along x - and y -directions computed using the following relations as

$$\lambda_1 = \frac{l_1}{l_0} \text{ and } \lambda_2 = \frac{l_2}{l_0} \quad (33)$$

Applying the deformation gradient (32), the invariants of the isochoric right Cauchy–Green deformation tensor, as defined in Eqs. (28) and (29), and the volume change $J = \det \mathbf{F}$ take the following form as

$$I'_1 = (\lambda_1^2 + \lambda_2^2 + 1) (\lambda_1 \lambda_2)^{-\frac{2}{3}} \quad (34)$$

$$I'_2 = (\lambda_1^2 \lambda_2^2 + \lambda_1^2 + \lambda_2^2) (\lambda_1 \lambda_2)^{-\frac{4}{3}} \quad (35)$$

$$J = \lambda_1 \lambda_2 \quad (36)$$

The strain energy function defined in Eqs. (30) and (31) together with the invariants of Eqs. (34)–(36) are used to learn the polynomial material model via the application of the fitting procedure.

4. Atomistic and continuum results

In order to determine the mechanical properties of epoxy/graphene nano-composite at nanoscale, three RVEs containing 1, 2 and 3 layers of graphene sheets are considered. Fig. 2 depicts the structure of the RVEs containing different layers of graphene sheets. Uniaxial and shear loadings are applied to each RVE by imposing appropriate deformation modes to the boundaries of the specified RVE by homogeneous deformation gradients. During atomistic simulations, the NVT ensemble is employed to keep the number of atoms, the volume of specimens and the temperature constant. The stress–strain curves obtained from

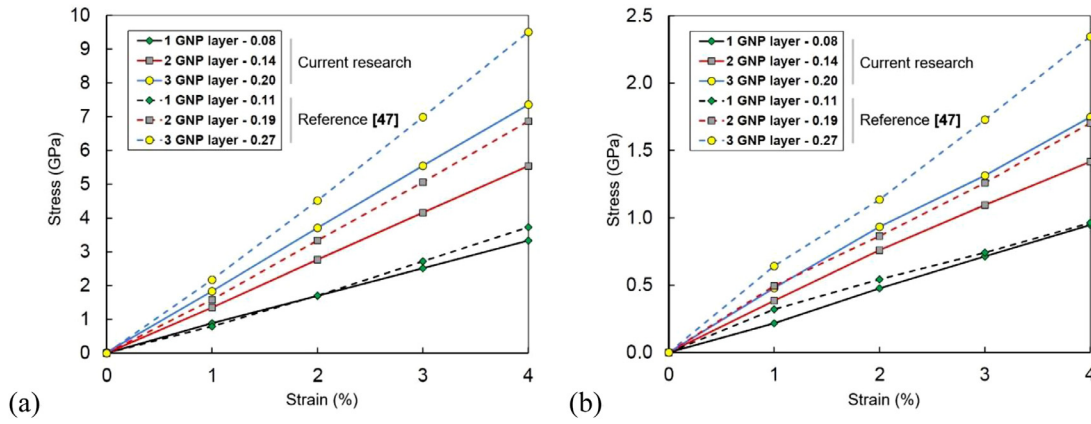


Fig. 3. Evolutions of stress–strain response of graphene/epoxy nano-composites including a multilayer of graphene nanoplate with indicated GNP volume fraction; (a) uniaxial deformation, (b) shearing deformation.

uniaxial deformation in x -direction and shearing deformation in xy -plane are shown in Fig. 3(a). It is evident from the graphs of this figure that the magnitude of stress that can be tolerated at a given strain value increases by increasing the number of graphene sheets. The results of Fig. 3(a) can be compared with those given in Fig. 3(b) that corresponds to Ref. [47] for a stiffness ratio of epoxy to graphene between 0.002 and 0.003. According to the results presented here, a specimen with one layer of graphene sheet can tolerate a stress magnitude up to 3.5GPa at a uniaxial strain of 4%, while based on Ref. [47], a similar specimen tolerates a stress of 3.8GPa for the same value of strain. On the other hand, for a specimen with two layers of graphene sheets, the maximum stress that is attained for the aforementioned value of strain is 5.5 GPa. This value is about 19% lower than the maximum stress of 6.8 GPa as obtained in Ref. [47]. However, it should be noted that the GNP volume fraction for the specimen with two GNP layers in current research is 0.14, while for a similar specimen in Ref. [47] it is 0.187. The GNP volume fraction and elastic modulus are compared in Table 2 for different specimens in current research and the corresponding specimens from Ref. [47]. The difference between the maximum values of stress is attributable to several factors; the type of potential employed in simulations, temperature at which the simulations are accomplished, strain rate and the GNP volume fraction (v_{GNP}) are among the important factors that can greatly influence the results. Especially, the GNP volume fraction has an essential role on elastic properties of GNP/epoxy composite. The densification procedure, as described in Section 2, is employed to properly model the epoxy and its effect on graphene sheets. Also, the MD simulations accomplished to determine the mechanical properties of graphene sheets are in good agreement with other studies [48–50]. These observations verify the accuracy of the RVEs that are employed to determine the mechanical characteristics of epoxy/graphene composites.

In order to link the nano-scale information to the continuum model, the stress data of RVEs are used to generate the stress surfaces. The stress surfaces are utilized to obtain exhaustive response of the material, which includes uniaxial, eq-biaxial, pure shear deformations and, also, data with different strain points. On the atomic side, the stress surfaces of atomic specimens are achieved by applying biaxial deformation to the RVEs. To this end, a strain amplitude of 30% is applied to obtain the reference data of atomistic structures, while the NVT ensemble has been used for the MD simulation. The reference data points of the MD simulations are illustrated for nano-composites including a graphene multilayer nano plate in Figs. 4 and 5. On the continuum side, the

Table 1

The material parameters (GPa) of hyperelastic function for multilayer graphene reinforced epoxy nano-composites.

| | 1 GNP layer | 2 GNP layers | 3 GNP layers |
|----------|-------------|--------------|--------------|
| C_{10} | 56.21 | 104.6 | 140.8 |
| C_{20} | -13.39 | -26.08 | -36 |
| C_{30} | 16.08 | 23.77 | 32.47 |
| C_{01} | -44.4 | -86.44 | -116.7 |
| C_{02} | 19.14 | 40.52 | 53.88 |
| C_{03} | -22.12 | -39.33 | -51.56 |
| K_1 | 1893 | 2339 | 2702 |
| K_2 | -761.4 | -1027 | -1245 |
| K_3 | -4632 | -5913 | -6946 |
| K_4 | 3530 | 4644 | 5545 |

Table 2

GNP volume fraction and elastic moduli for specimens containing different number of GNP layers and 80% crosslink density.

| | v_{GNP} | E (GPa) | |
|--------------|-----------|------------------|-----------|
| | | Current research | Ref. [47] |
| 1 GNP layer | 0.077 | 0.111 | 82 |
| 2 GNP layers | 0.14 | 0.187 | 134.25 |
| 3 GNP layers | 0.20 | 0.271 | 179.75 |

polynomial hyperelastic model is used to develop the homogenized strain energy function for nonlinear analysis. The first order derivative of the hyperelastic function with respect to the right Cauchy–Green deformation tensor is calculated for the stress components of the continuum model using Eq. (30). Furthermore, the σ_x and σ_y components of the Cauchy-stress response of hyperelastic function are least squares fitted to the 121 data points of atomistic stresses in biaxial deformation. The material parameters of the fitted hyperelastic function are presented in Table 1. At this point, it is worth mentioning that the stress surfaces are fitted to the atomistic data whose validity is confirmed as discussed previously. These stress surfaces are then employed for the multiscale analysis of specimens at microscale. Consequently, many factors that may influence the results of MD simulations, such as the rate of loading, are naturally excluded from the analysis. In this sense, it can be concluded that the multi-scale analyses are quasi-static.

In Fig. 4, the generated surfaces for σ_x component approximate the atomistic data with sufficient accuracy. It is evident from the stress surfaces that the stress response of nano-composites increases by increasing the number of graphene layers. The maximum value of σ_x for an RVE containing one graphene layer is

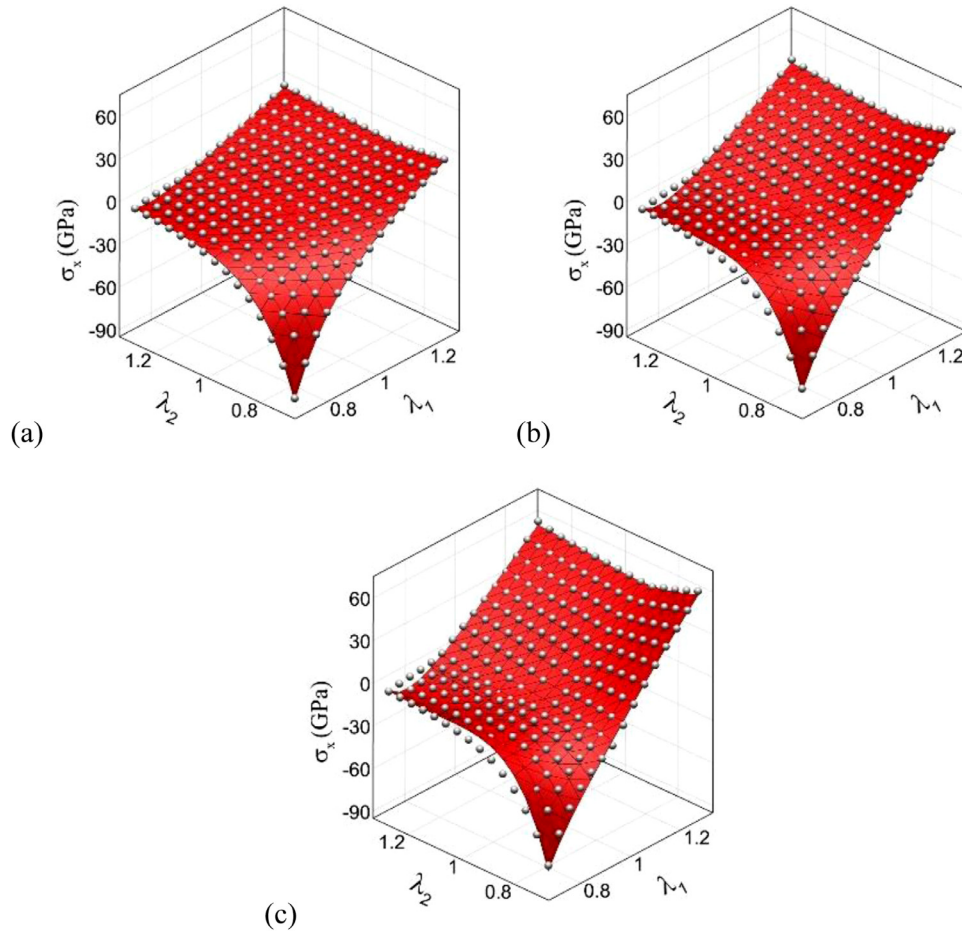


Fig. 4. Atomistic (spherical) and continuum (surface) stress σ_x response of graphene/epoxy nano-composites; (a) 1 GNP layer, (b) 2 GNP layers and (c) 3 GNP layers.

around 25GPa, while this value increases to 60GPa for an RVE that contains 3 layers of graphene sheets. The surfaces for σ_y component of Cauchy-stress are shown in Fig. 5. Clearly, satisfactory coincidence can be observed between the generated surfaces and atomistic data. The results of Figs. 4 and 5 clearly indicate that the hyperelastic function is capable of describing the behavior of multilayer graphene reinforced epoxy nano-composites. It must be noted that the main goal of this research is to develop an efficient hierarchical multiscale technique to determine the nonlinear mechanical behavior of graphene/epoxy nano-composites. The mechanical properties of pure epoxy are highly dependent on temperature. The temperature of 1K has been majorly selected to avoid the necessity for replicating time consuming MD simulations for different temperature levels. In other words, to account for the effect of temperature, it is only necessary to set the temperature to desired value and perform the atomistic simulations for that value. The stress surfaces that are generated for new value of temperature can then be used for the multiscale analysis of different specimens. To accomplish the multi-scale analysis, it is necessary to discretize the continuum at upper scale (microscale) using conventional finite elements. The Gauss points of these elements lie in the RVEs at lower scale (nanoscale), where the stress and elasticity tensor are computed using the generated stress surfaces as discussed above. In fact, the necessity for time consuming MD simulations for the RVEs at lower scale is eliminated by the application of stress surfaces that represent the behavior of nanoscale RVEs

subject to uniaxial, eq-biaxial and shear loading conditions. The boundary conditions for the RVEs in lower scale are specified by the homogenous deformation gradients that are computed at the Gauss points of finite elements at upper scale. On the other hand, the stress and elasticity tensor that are required to compute element stresses and internal forces are obtained from the RVEs at lower scale.

5. Multi-scale simulation results

In order to illustrate the performance and applicability of proposed multi-scale method, different numerical examples are presented here. In all of these examples, the continuum at microscale is discretized using finite elements, the Gauss points of which lie in the RVEs at nano-scale. It is assumed that the properties of the continuum in upper scale coincides with the properties of the RVEs along xy - plane in lower scale. The nonlinear behavior of the materials is implemented into the model through the elasticity tensor, which is obtained from the strain energy function described in previous sections. The integration points of elements inherit the nonlinear characteristic of RVEs using the hyperelastic model. The stress-strain response of the MD simulation is compared in Fig. 6 with a single element response of the FEM to indicate the accuracy of implemented hyperelastic function. Furthermore, the influence of multilayer graphene sheets in nano-composites is investigated by two multi-scale examples.

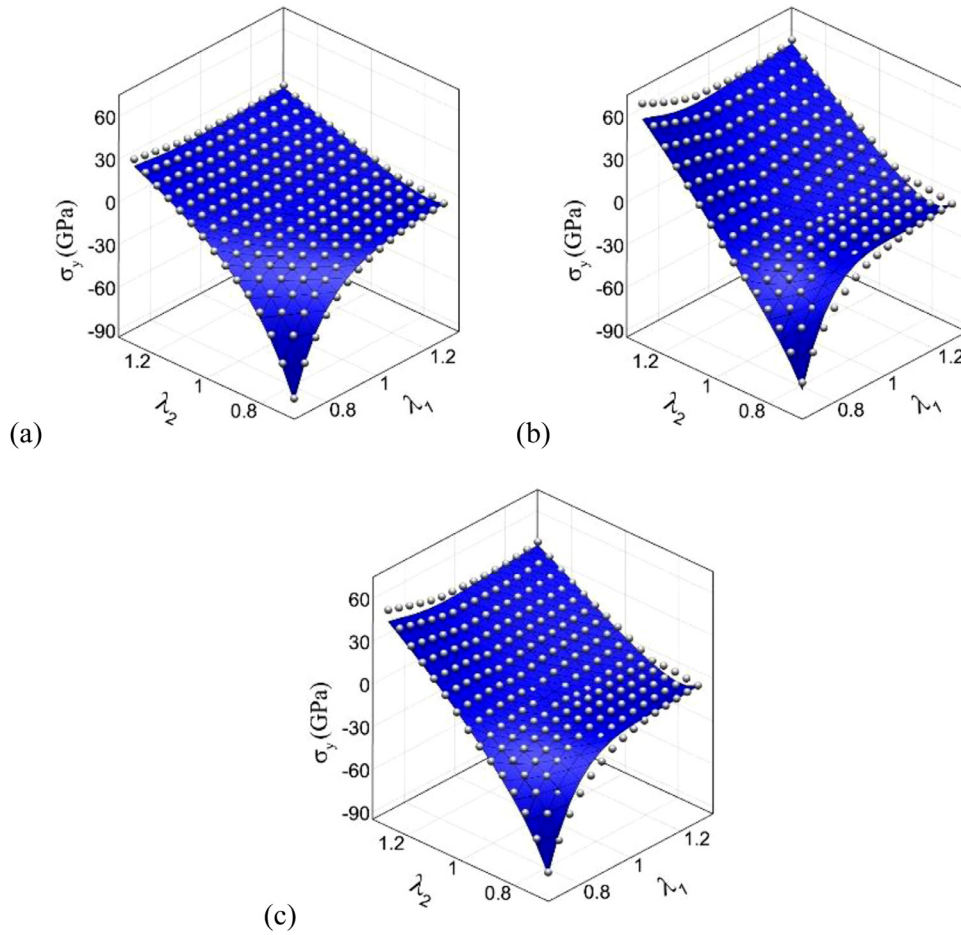


Fig. 5. Atomistic (spherical) and continuum (surface) stress σ_y response of graphene/epoxy nano-composites; (a) 1 GNP layer, (b) 2 GNP layers and (c) 3 GNP layers.

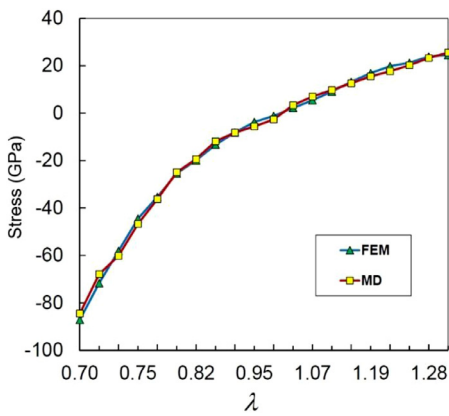


Fig. 6. Evolution of stress-strain response of graphene/epoxy nano-composites under biaxial deformation.

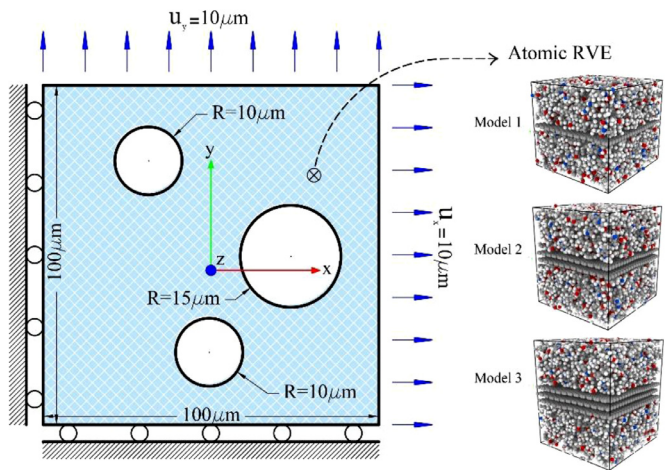


Fig. 7. A perforated plate under biaxial deformation.

5.1. Perforated plate under biaxial deformation

In the first numerical example, a biaxial deformation is applied to the free edges of a perforated square plate with a length of $100\mu\text{m}$ along principal directions. The plate includes three randomly distributed holes with radii of 10 and $15\mu\text{m}$. A tensile de-

formation of $10\mu\text{m}$ is applied to the top and right edges of the plate using 50 load steps, while the bottom and left edges remain fixed. Fig. 7 displays the geometry of specimen. A fine finite element mesh is used to ensure that the discretization error can

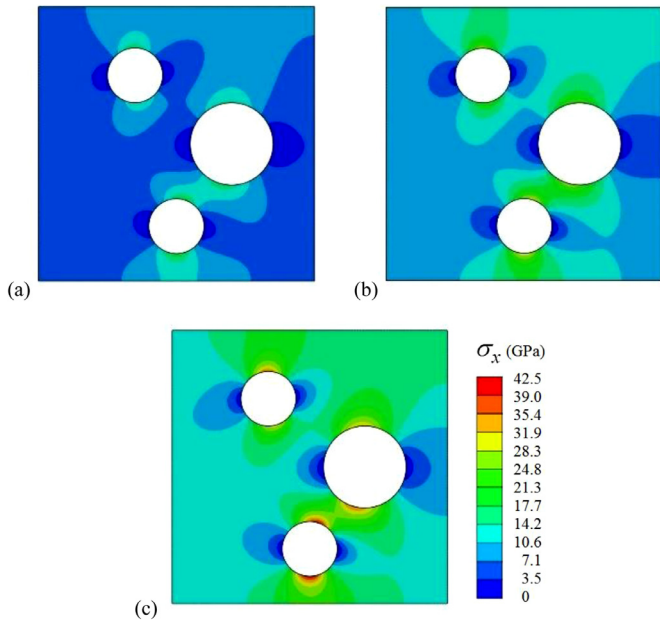


Fig. 8. The stress σ_x contours of the perforated plate of graphene/epoxy nano-composites under biaxial deformation; (a) 1 GNP layer, (b) 2 GNP layers and (c) 3 GNP layers.

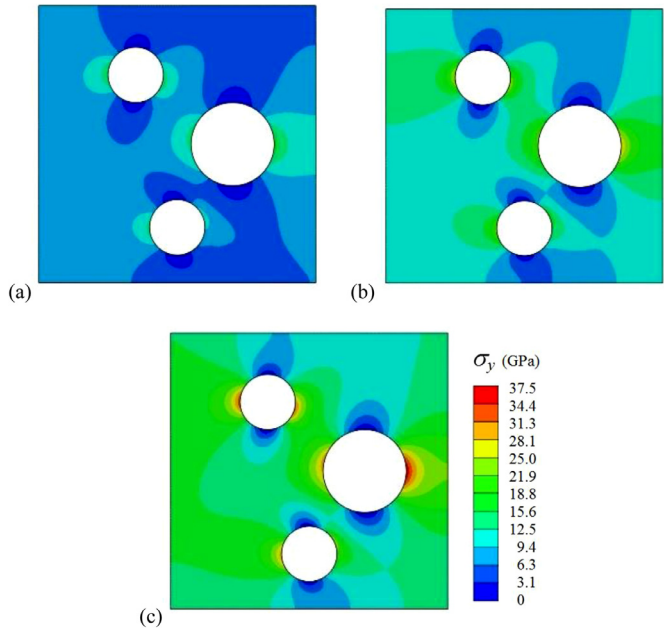


Fig. 9. The stress σ_y contours of the perforated plate of graphene/epoxy nano-composites under biaxial deformation; (a) 1 GNP layer, (b) 2 GNP layers and (c) 3 GNP layers.

be neglected in comparison with the model error. Quadratic elements with four Gauss points are employed and plane strain conditions are assumed. The material properties used for the atomistic simulation are specified for each integration point through the stress and elasticity tensors of associated hyperelastic function in lower scale. The numerical example is solved for multilayer graphene/epoxy nano-composites based on the finite element method.

The Cauchy stress contours of the perforated plate under biaxial deformation using the material properties of different RVEs are shown in Figs. 8–10. The results indicate that the stress in the specimen increases by increasing the number of graphene sheets that can be expected as the material becomes stiffer. In order to investigate the influence of different numbers of graphene sheets on the mechanical response of the plate, the stress components σ_x and σ_y are plotted along the vertical line $x = 0$ and horizontal line $y = 0$. The variations of stress components along the vertical and horizontal lines are presented in Fig. 11. Based on the curves of this figure, it can be observed that the maximum value of σ_x occurs at the left and right edges of circles, especially the larger circle. Similarly, the stress component σ_y takes its maximum at the top and bottom edges of circles. It is clear that the maximum values of stress components increase by increasing the number of graphene sheets accordingly.

5.2. Ring under tensile deformation

In the second example, a ring with an internal and external radii of 30 and 40 μm , subject to a prescribed displacement, is studied. A tensile deformation of 15 μm along x -direction is exerted onto the right edge of the ring, while the left edge is fixed in this direction, as shown in Fig. 12. In order to model the ring, quadratic elements with four Gauss points per element are employed and plane strain conditions are assumed. Each integration point of finite element model in micro-scale lies in the RVE in

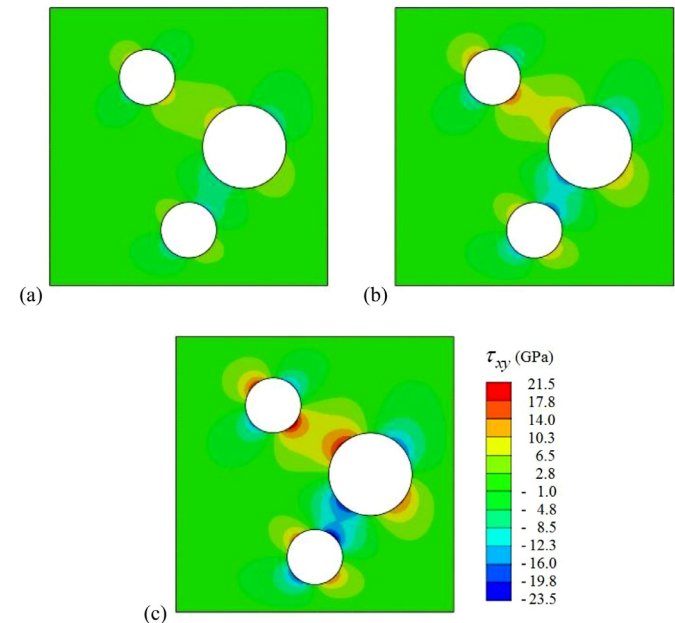


Fig. 10. The stress τ_{xy} contours of the perforated plate of graphene/epoxy nano-composites under biaxial deformation; (a) 1 GNP layer, (b) 2 GNP layers and (c) 3 GNP layers.

nano-scale; the stress components and elasticity tensors are computed via the application of hyperelastic function and its material constants and sent back to the Gauss points in upper scale. In order to illustrate the effect of multilayer graphene sheets on the overall response of the model, RVEs including one, two and three graphene nano-plates are selected.

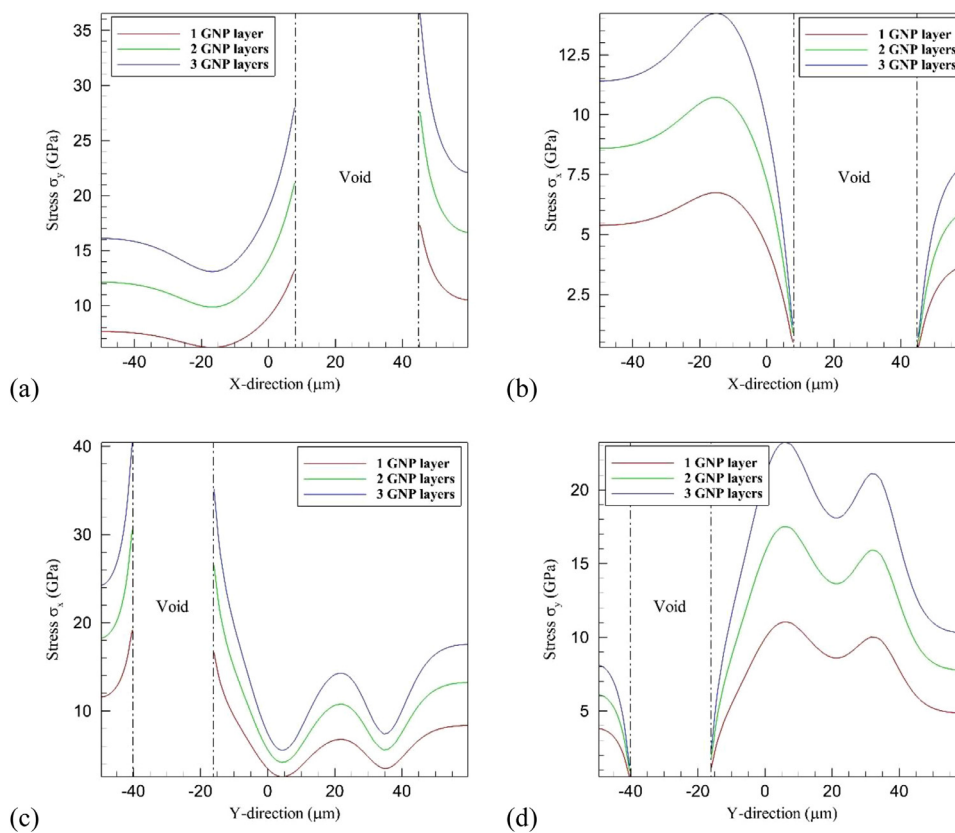


Fig. 11. The evaluation of stress components along the horizontal and vertical lines passing through the center of perforated plate.

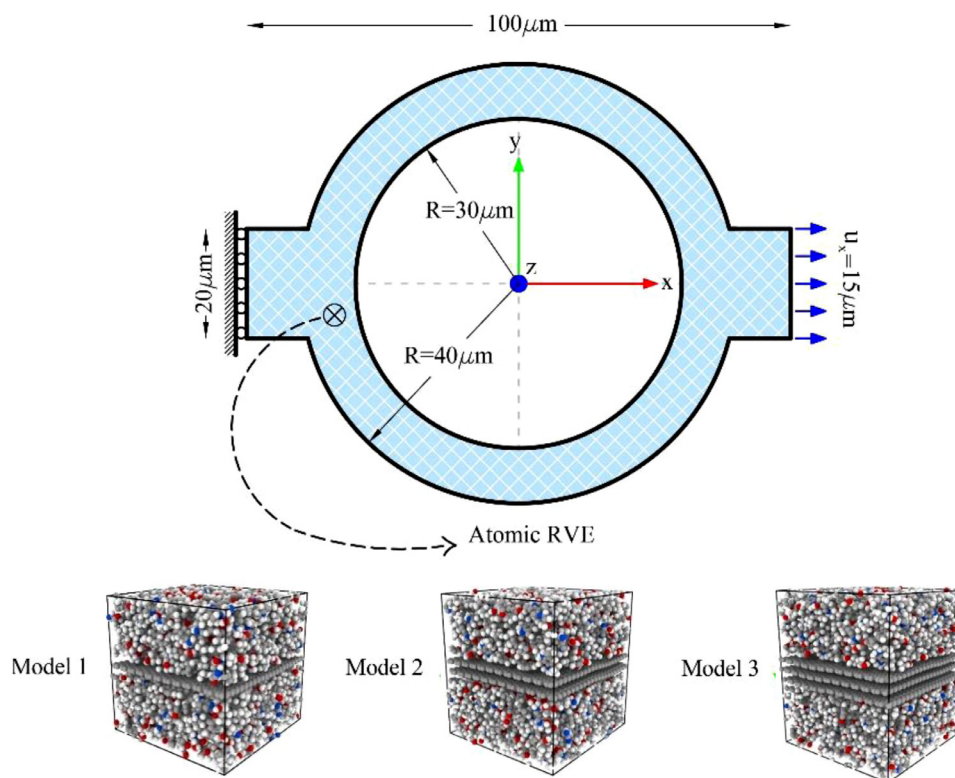


Fig. 12. A ring under tensile deformation.

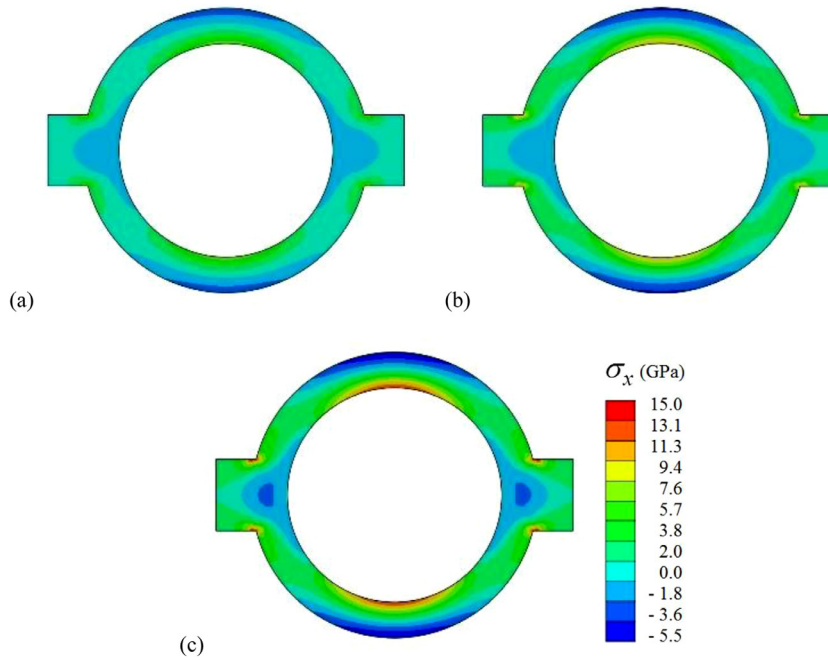


Fig. 13. The stress σ_x contours of the ring of graphene/epoxy nano-composites under tensile deformation; (a) 1 GNP layer, (b) 2 GNP layers and (c) 3 GNP layers.

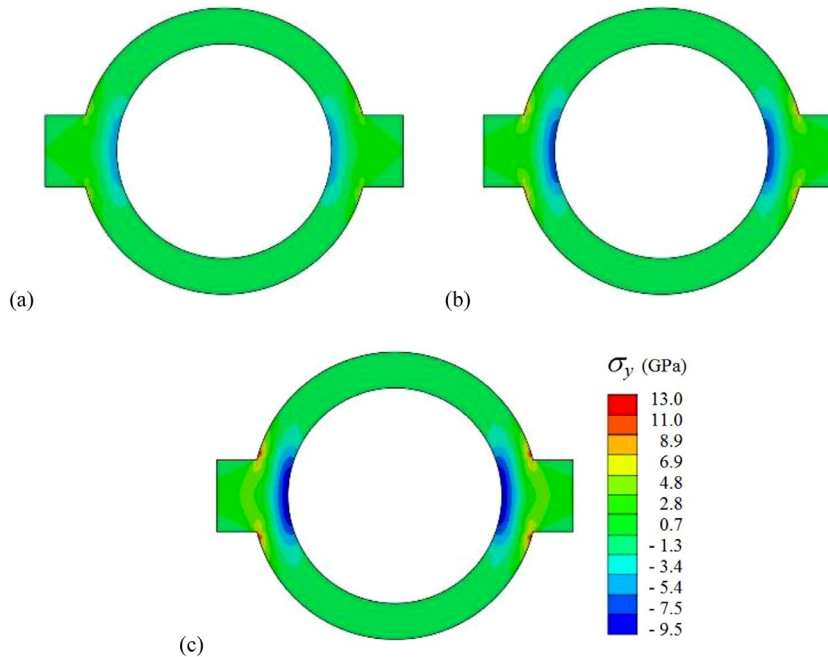


Fig. 14. The stress σ_y contours of the ring of graphene/epoxy nano-composites under tensile deformation; (a) 1 GNP layer, (b) 2 GNP layers and (c) 3 GNP layers.

In order to demonstrate the applicability of proposed hyperelastic functions, the contours of stress components σ_x and σ_y for epoxy embedded with multilayer graphene sheets are presented in Figs. 13 and 14, respectively. Numerical results confirm that increasing the number of graphene sheets increases the overall stiffness of the ring. Furthermore, the force-displacement response of the model are plotted in Fig. 15 to indicate the effect of dif-

ferent number of GNP layers on the behavior of specimen. The displacement-control approach is applied to the model under tensile deformation. The graphs of Fig. 15 present that the force response increases by increasing the number of GNP in the model. The results clearly highlight that the proposed hyperelastic function is capable of reproducing the structural behavior at atomistic level without the need for using complex interatomic potential.

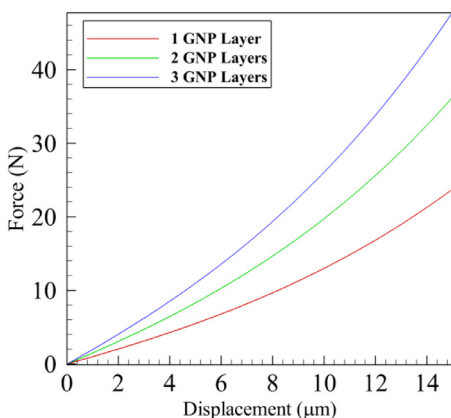


Fig. 15. The force-displacement curves of graphene/epoxy nano-composites under tensile deformation.

6. Conclusion

In the present paper, a multi-scale technique was proposed to connect the atomistic information to the continuum models. The mechanical behavior of graphene/epoxy nano-composites was studied based on the molecular dynamics analysis. Due to the high computational cost of MD simulation, the multi-scale method was developed for modeling the behavior of nano-composites by using the stress response surfaces of RVEs and linking it with a continuum model. It was discussed that utilizing the stress surface of atomistic simulation can be an effective data in order to obtain a hyperelastic function for complex nano-structures and highly decrease the computational expenses for multi-scale analysis. By employing this approach, the strain energy density, stress and material elasticity tensors of nano-composites can be directly derived from the hyperelastic function. Also, the aforementioned function can be easily implemented in finite element analysis without using complex interatomic information. In order to generate the stress surfaces of atomistic simulation, the biaxial loading was subjected to the RVEs. Applying the least square method, the hyperelastic function was fitted to the atomic data and the material constants were obtained for the hyperelastic model. The influence of graphene on the material behavior of graphene/epoxy nano-composites was investigated for multilayer graphene sheets. In order to illustrate the efficiency of the proposed multi-scale technique, the finite element method was employed to solve numerical examples at a larger-scale in which the integration points inherit the material properties from RVE at a smaller-scale. It was illustrated that increasing the number of graphene sheets increases the mechanical response of graphene/epoxy nano-composites. The numerical results, as presented in this work, clearly show the efficiency and applicability of the proposed multi-scale technique.

Declaration of Competing Interest

None.

References

- [1] P. Chowdhury, H. Sehitoglu, R. Rateick, Damage tolerance of carbon-carbon composites in aerospace application, *Carbon* 126 (2018) 382–393.
- [2] N. Li, Y. Li, J. Jelonnek, G. Link, J. Gao, A new process control method for microwave curing of carbon fibre reinforced composites in aerospace applications, *Compos. Part B: Eng.* 122 (2017) 61–70.
- [3] L. Kong, X. Zuo, S. Zhu, Z. Li, J. Shi, L. Li, Z. Feng, D. Zhang, D. Deng, J. Yu, Novel carbon-poly (silacetylene) composites as advanced thermal protection material in aerospace applications, *Compos. Sci. Technol.* 162 (2018) 163–169.
- [4] J. Wei, T. Vo, F. Inam, Epoxy/graphene nanocomposites – processing and properties: a review, *RSC Adv.* 5 (2015) 73510–73524.
- [5] L.C. Tang, Y.J. Wan, D. Yan, Y.B. Pei, L. Zhao, Y.B. Li, L.B. Wu, J.X. Jiang, G.Q. Lai, The effect of graphene dispersion on the mechanical properties of graphene/epoxy composites, *Carbon* 60 (2013) 16–27.
- [6] J.A. King, D.R. Klimek, I. Miskioglu, G.M. Odegard, Mechanical properties of graphene nanoplatelet/epoxy composites, *J. Compos. Mater.* 49 (2015) 659–668.
- [7] T. Kuilla, S. Bhadra, D. Yao, N.H. Kim, S. Bose, J.H. Lee, Recent advances in graphene based polymer composites, *Prog. Polym. Sci.* 35 (2010) 1350–1375.
- [8] O. Aluko, S. Gowtham, G. Odegard, Multiscale modeling and analysis of graphene nanoplatelet/carbon fiber/epoxy hybrid composite, *Compos. Part B: Eng.* 131 (2017) 82–90.
- [9] S. Sharma, R. Chandra, P. Kumar, N. Kumar, Molecular dynamics simulation of polymer/carbon nanotube composites, *Acta Mech. Solida Sin.* 28 (2015) 409–419.
- [10] R. Chawla, S. Sharma, Molecular dynamics simulation of carbon nanotube pull-out from polyethylene matrix, *Compos. Sci. Technol.* 144 (2017) 169–177.
- [11] A. Pedrielli, S. Taioli, G. Garberoglio, N.M. Pugno, Mechanical and thermal properties of graphene random nanofoams via molecular dynamics simulations, *Carbon* 132 (2018) 766–775.
- [12] J. Moon, S. Yang, M. Cho, Interfacial strengthening between graphene and polymer through stone-thrower-wales defects: ab initio and molecular dynamics simulations, *Carbon* 118 (2017) 66–77.
- [13] G. Chen, A. Li, H. Liu, S. Huang, Z. Zhang, W. Liu, C. Zha, B. Li, Z. Wang, Mechanical and dynamic properties of resin blend and composite systems: a molecular dynamics study, *Compos. Struct.* 190 (2018) 160–168.
- [14] Y. Qiu, Y. Zhang, A. Ademiloye, Z. Wu, Molecular dynamics simulations of single-layer and rotated double-layer graphene sheets under a high velocity impact by fullerene, *Comput. Mater. Sci.* 182 (2020) 109798.
- [15] S.T. Oyinbo, T.C. Jen, Molecular dynamics investigation of temperature effect and surface configurations on multiple impacts plastic deformation in a palladium-copper composite metal membrane (CMM): a cold gas dynamic spray (CGDS) process, *Comput. Mater. Sci.* 185 (2020) 109968.
- [16] J. Xi, G. Bokas, L. Schultz, M. Gao, L. Zhao, Y. Shen, J. Perepezko, D. Morgan, I. Szlufarska, Microalloying effect in ternary Al-Sm-X (X = Ag, Au, Cu) metallic glasses studied by ab initio molecular dynamics, *Comput. Mater. Sci.* 185 (2020) 109958.
- [17] M. Jahanshahi, A.R. Khoei, N. Jafarian, N. Heidarzadeh, An atomistic-continuum multiscale method for modeling the thermomechanical behavior of heterogeneous nanostructures, *Int. J. Multiscale Comput. Eng.* 16 (2018) 441–464.
- [18] R. Rahman, A. Haque, Molecular modeling of crosslinked graphene-epoxy nanocomposites for characterization of elastic constants and interfacial properties, *Compos. Part B: Eng.* 54 (2013) 353–364.
- [19] S.C. Shiu, J.L. Tsai, Characterizing thermal and mechanical properties of graphene/epoxy nano-composites, *Compos. Part B: Eng.* 56 (2014) 691–697.
- [20] C. Li, A.R. Browning, S. Christensen, A. Strachan, Atomistic simulations on multilayer graphene reinforced epoxy composites, *Compos. Part A: Appl. Sci. Manuf.* 43 (2012) 1293–1300.
- [21] M. Li, H. Zhou, Y. Zhang, Y. Liao, H. Zhou, Effect of defects on thermal conductivity of graphene/epoxy nanocomposites, *Carbon* 130 (2018) 295–303.
- [22] L. Shilkrot, W. Curtin, R. Miller, A coupled atomistic/continuum model of defects in solids, *J. Mech. Phys. Solids* 50 (2002) 2085–2106.
- [23] W. Liu, E. Karpov, S. Zhang, H. Park, An introduction to computational nanomechanics and materials, *Comput. Methods Appl. Mech. Eng.* 193 (2004) 1529–1578.
- [24] J. Ericksen, On the Cauchy–Born rule, *Math. Mech. Solids* 13 (2008) 199–220.
- [25] A.R. Khoei, M. Jahanshahi, Multi-scale modeling of plastic deformations in nano-scale materials; transition to plastic limit, *Int. J. Numer. Methods Eng.* 109 (2017) 1180–1216.
- [26] E.B. Tadmor, M. Ortiz, R. Phillips, Quasicontinuum analysis of defects in solids, *Philos. Mag. A* 73 (1996) 1529–1563.
- [27] L. Beex, O. Roko’s, J. Zeman, S. Bordas, Higher-order quasicontinuum methods for elastic and dissipative lattice models: uniaxial deformation and pure bending, *GAMM – Mitteilungen* 38 (2015) 344–368.
- [28] G.J. Wagner, W.K. Liu, Coupling of atomistic and continuum simulations using a bridging scale decomposition, *J. Comput. Phys.* 190 (2003) 249–274.
- [29] R.E. Rudd, J.Q. Broughton, Coarse-grained molecular dynamics and the atomic limit of finite elements, *Phys. Rev. B* 58 (1998) R5893–R5896.
- [30] A.R. Khoei, M.J.A. Qomi, M. Kazemi, A. Aghaei, An investigation on the validity of Cauchy–Born hypothesis using Sutton–Chen many-body potential, *Comput. Mater. Sci.* 44 (2009) 999–1006.
- [31] A. Shahabodini, R. Ansari, M. Darvizeh, Multiscale modeling of embedded graphene sheets based on the higher order Cauchy–Born rule: nonlinear static analysis, *Compos. Struct.* 165 (2017) 25–43.
- [32] A.R. Khoei, M. Jahanshahi, G. Toloui, Validity of Cauchy–Born hypothesis in multi-scale modeling of plastic deformations, *Int. J. Solids Struct.* 115–116 (2017) 224–247.
- [33] A.K. Shojaei, P. Volgers, A coupled hyperelastic-plastic-continuum damage model for studying cyclic behavior of unfilled engineering polymers, *Int. J. Fatigue* 107 (2018) 33–39.
- [34] V. Zamani, T.J. Pence, H. Demirkoparan, H. Topol, Hyperelastic models for the swelling of soft material plugs in confined spaces, *Int. J. Non Linear Mech.* 106 (2018) 297–309.
- [35] A. Kossa, S. Berezvzi, Novel strategy for the hyperelastic parameter fitting procedure of polymer foam materials, *Polym. Test* 53 (2016) 149–155.

- [36] M. Jahanshahi, H. Ahmadi, A.R. Khoei, A hierarchical hyperelastic-based approach for multi-scale analysis of defective nano-materials, *Mech. Mater.* 140 (2020) 103206.
- [37] E. Saavedra Flores, S. Adhikari, M. Friswell, F. Scarpa, Hyperelastic axial buckling of single wall carbon nanotubes, *Phys. E: Low-Dimens. Syst. Nanostruct.* 44 (2011) 525–529.
- [38] M. Arroyo, T. Belytschko, An atomistic-based finite deformation membrane for single layer crystalline films, *J. Mech. Phys. Solids* 50 (2002) 1941–1977.
- [39] E. Saavedra Flores, S. Adhikari, M. Friswell, F. Scarpa, Hyperelastic finite element model for single wall carbon nanotubes in tension, *Comput. Mater. Sci.* 50 (2011) 1083–1087.
- [40] E. Saavedra Flores, R. Ajaj, S. Adhikari, I. Dayyani, M. Friswell, R. Castro-Triguero, Hyperelastic tension of graphene, *Appl. Phys. Lett.* 106 (2015) 061901.
- [41] W. Kim, H. Chung, M. Cho, Anisotropic hyperelastic modeling for face-centered cubic and diamond cubic structures, *Comput. Methods Appl. Mech. Eng.* 291 (2015) 216–239.
- [42] M. Jahanshahi, A.R. Khoei, N. Heidarzadeh, N. Jafarian, A hierarchical thermo-mechanical multi-scale technique for modeling of edge dislocations in nano-crystalline structures, *Comput. Mater. Sci.* 141 (2018) 360–374.
- [43] H. Ahmadi, M. Hajikazemi, W. van Paepegem, Closed-form formulae for prediction of homogenized plyproperties and laminate thermo-elastic constants in symmetric laminates containing ply cracks in multiple orientations, *Compos. Struct.* 241 (2020) 112061.
- [44] M. Hajikazemi, L. McCartney, H. Ahmadi, W. van Paepegem, Variational analysis of cracking in general composite laminates subject to triaxial and bending loads, *Compos. Struct.* 239 (2020) 111993.
- [45] H. Sun, Compass: an ab initio force-field optimized for condensed-phase applications overview with details on alkane and benzene compounds, *J. Phys. Chem. B* 102 (1998) 7338–7364.
- [46] S. Plimpton, Fast parallel algorithms for short-range molecular dynamics, *J. Comput. Phys.* 117 (1995) 1–19.
- [47] C. Hadden, D. Klimek-McDonald, E. Pineda, J. King, A. Reichanadter, I. Miskioglu, S. Gowtham, G. Odegard, Mechanical properties of graphene nanoplatelet/carbon fiber/epoxy hybrid composites: multiscale modeling and experiments, *Carbon* 95 (2015) 100–112.
- [48] S. Thomas, K.M. Ajith, S.U. Lee, M.C. Valsakumar, Assessment of the mechanical properties of monolayer graphene using the energy and strain-fluctuation methods, *RSC Adv.* 8 (2018) 27283–27292.
- [49] J.W. Jiang, J.S. Wang, B. Li, Young's modulus of graphene: a molecular dynamics study, *Phys. Rev. B* 80 (2009) 113405.
- [50] E. Cadelano, P.L. Palla, S. Giordano, L. Colombo, Nonlinear elasticity of monolayer graphene, *Phys. Rev. Lett.* 102 (2009) 235502.